Miner Deposita (2007) 42:89–105
DOI 10.1007/s00126-006-0110-6

ARTICLE

The Granites gold deposits, Northern Territory, Australia: evidence for an early syn-tectonic ore genesis

G. J. Adams · R. A. Both · P. James

Received: 1 January 2006 / Accepted: 25 October 2006 / Published online: 21 November 2006

Abstract The ore deposits of The Granites goldfield are shear-hosted within Palaeoproterozoic amphibolite facies metasedimentary rocks in the Tanami Region, Northern Territory, Australia. The ore bodies are located within a 5- to 35-m thick sequence of steeply dipping unit of metamorphosed iron-rich metasedimentary rocks. Deformation at The Granites was complex and is characterized by five successive deformation phases (D_{1-5}). Shear veins (central and oblique) are the dominant type of vein geometry, with minor development of extensional veins and reverse-fault related veins. Four generations of syn-tectonic veins, corresponding to D_1, D_3, D_4, and D_5, have been recognized and are comprised of quartz, quartz-carbonate, calc-silicate, and calcite. In addition, two generations of disseminated sulfide–arsenide mineralization, dominated by pyrrhotite, arsenopyrite, and loellingite, with minor pyrite, chalcopyrite and rare marcasite, formed syn-D_1 and syn- to post-D_3. Textural and structural evidence indicates deposition of gold was contemporaneous with the syn-D_1 veins and sulfide–arsenide mineralization. Four hydrothermal phases are proposed for the formation of the veins and disseminated sulfide–arsenide assemblages. The first phase (D_1) was responsible for transport and deposition of the majority of the gold. Minor remobilization and deposition of gold occurred during the D_3 and D_4 phases. Little is known about the nature of the D_1 ore fluid, although a relatively low sulfur content is indicated by the assemblage pyrrhotite–arsenopyrite–loellingite+rare pyrite. The growth of amphibolite facies metamorphic minerals andalusite and almandine garnet during D_1 indicates a high temperature for the fluid. The D_3 hydrothermal phase coincided with peak metamorphism. D_4 fluids were hypersaline, high temperature, CO_2-poor, and H_2S-poor.

Keywords Tanami region · Proterozoic gold · Structural control · Shear veins · Fluid inclusions · Sulfur isotopes

Editorial handling: L. Meinert

G. J. Adams · R. A. Both · P. James
School of Earth and Environmental Sciences,
University of Adelaide,
Adelaide, South Australia 5005, Australia

Present address:
G. J. Adams (✉)
Newmont, Jundee Operations,
P.O. Box 1652, Subiaco, Western Australia 6904, Australia
e-mail: garry.adams@newmont.com

Present address:
P. James
School of Natural and Built Environments,
University of South Australia,
Adelaide, South Australia 5005, Australia

Introduction

The Granites gold mine is situated within the Tanami Region in the Northern Territory, 550 km northwest of Alice Springs (Fig. 1). The deposits are hosted within polydeformed Palaeoproterozoic metasedimentary rocks that have been metamorphosed to amphibolite facies. Gold mineralization is found within veins and disseminated sulfides in the essentially stratabound main host unit, which is localized within a major shear zone. To the end of April 2002, 6.3 Mt at 5.5 g/t Au had been mined at The Granites (Fig. 1), producing 1.1 Moz of gold.

Previous studies of The Granites gold deposits have presented contrasting genetic models. Scrimgeour and Sandiford (1993) favored an early, high-temperature model, arguing that the influx of large amounts of fluid during

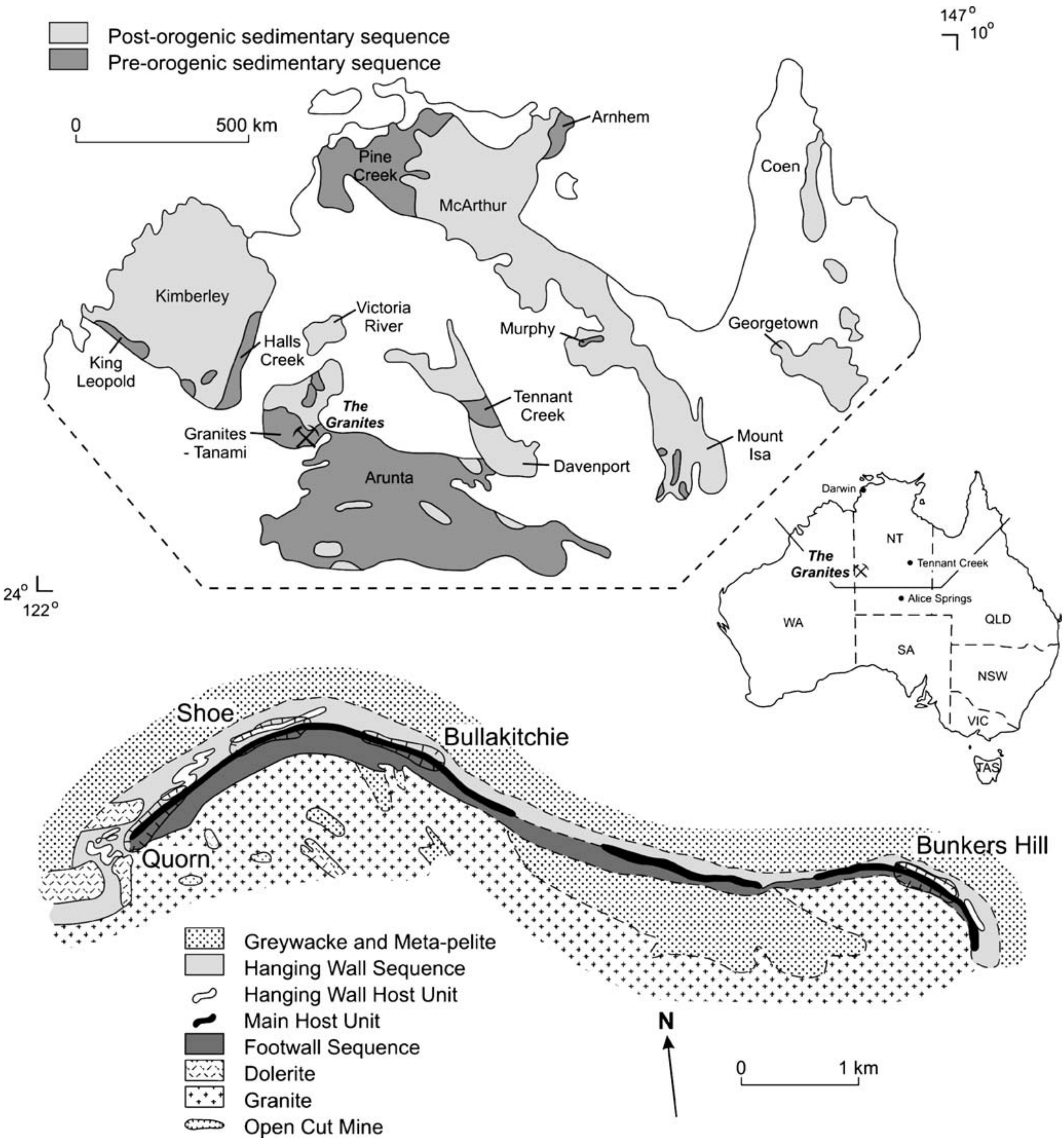

Fig. 1 Location diagram for The Granites gold mines, including a generalized map (*top*) of northern Australia showing the locations of the Palaeoproterozoic to Mesoproterozoic terranes and the distribution of pre-Barramundi Orogeny supracrustal sequences (modified from Page 1988), and The Granites gold mines (*bottom*)

deformation is consistent with the significant role that fluids play in the early stages of metamorphism. According to this model, influx of these fluids produced the metasomatism, gold mineralization, and extensive veining seen at The Granites. Valenta and Wall (1996) also advocated an early, high-temperature model and contended that the high-temperature metamorphism was a consequence of granites intruding the regionally metamorphosed stratigraphic package. They also argued that the mineralization has been largely overprinted by later deformation, implying that the present geometry of mineralization is different to the likely original geometry. On the other hand, Vandenberg et al. (2001) and Wygralak et al. (2001) favored a late, low-temperature model for The Granites deposits. Both Vandenberg et al.

(2001) and Wygralak et al. (2001) argued that late structures are the most important controls on the gold mineralization, implying a lower temperature deposition of gold late in the tectonic evolution of the region. In this paper, we present evidence to further support an early, high-temperature syn-tectonic model for ore genesis at The Granites.

Regional geology

The Tanami Region is bordered by the Palaeoproterozoic Arunta Inlier to the southeast, the Mesoproterozoic to Neoproterozoic Birrindudu Basin to the north and west, and the Cambrian Wiso Basin to the east (Fig. 1). The oldest exposed rocks in the Tanami Region are isolated inliers of Archaean gneiss and schist with protolith ages of 2,510 Ma (Page et al. 1995). The orogenic sequences that overlie these Archaean inliers comprise the Tanami Group, the Ware Group, and the Mount Charles Formation (Crispe et al. 2006), which are multiply-deformed volcanic and sedimentary rocks. The Tanami Group consists of the Dead Bullock Formation and the turbiditic Killi Killi Formation (Vandenberg et al. 2001). The Granites gold deposits are hosted within the Dead Bullock Formation, which consists of graphitic shale, carbonaceous siltstone, minor iron-rich BIF, and chert. The Tanami Event terminated Tanami Group sedimentation between 1,845 and 1,830 Ma (Vandenberg et al. 2001). The Tanami Event is younger than the widespread Barramundi Orogeny, a major orogenic event that deformed central and northern Australia between 1,880 and 1,850 Ma (Etheridge et al. 1987; Page 1988). The Tanami Group was overlain by volcanic and sedimentary rocks of the Mount Charles Formation and intruded by post-tectonic granitoids including The Granites Granite. The Tanami Event and the overprinting by subsequent tectonic events make interpretation of the early evolution of the region difficult. The layered rocks of the Tanami Group are generally steeply dipping, usually with a bedding parallel schistosity.

Local geology

The Granites gold deposits occur over a 9-km strike length (Fig. 1) and consist of four open cut mines [Quorn, Shoe, Bullakitchie (East and West), and Bunkers Hill] and two underground mines (Shoe and East Bullakitchie). East Bullakitchie has produced the highest grade ore, with the gold hosted within quartz, quartz-carbonate, and calc-silicate veins. The other deposits at Quorn, Shoe, West Bullakitchie, and Bunkers Hill differ from East Bullakitchie as the gold is hosted predominantly within sulfide disseminations. The Dead Bullock Formation (previously the Mount Charles Beds) at The Granites has been informally subdivided into the footwall sequence (FWS), the main host unit (MHU), and the hanging wall sequence (HWS) (Ireland and Mayer 1984; Mayer 1990). There is no evidence of gross repetition of these units throughout the 9-km strike length at The Granites.

The metasedimentary rocks at The Granites have been affected by amphibolite facies metamorphism, as indicated by the presence of andalusite, cummingtonite, almandine garnet, gedrite, cordierite, hornblende, and sillimanite. Scrimgeour and Sandiford (1993) interpreted that peak P–T conditions, as defined in pelitic schists by a prograde biotite–andalusite–sillimanite–garnet assemblage, developed near the end of deformation. Using, this assemblage, THERMCALC and garnet–biotite geothermometry, Scrimgeour and Sandiford (1993) estimated peak metamorphic conditions at 600°C and 3.5 kbar. In semi-pelitic schists, they documented an early prograde assemblage of biotite–garnet±cordierite that was overprinted by a late prograde assemblage of unoriented gedrite-cordierite. This latter assemblage was used as evidence for high temperature metasomatism. According to Scrimgeour and Sandiford (1993), peak metamorphic conditions occurred during their D_2, which corresponds to D_3 of this study (see below), the last major deformation event to affect rocks at The Granites. The peak metamorphic assemblage in pelitic schists was overprinted by retrograde staurolite–chlorite–muscovite assemblage, which indicates temperatures of 550–560°C (Scrimgeour and Sandiford 1993). Despite the metamorphic grade and intense deformation, some of the rocks preserve original sedimentary textures and structures.

Intrusive rocks at The Granites represent a long time frame of igneous activity. Some intrusions are highly schistose and fractured, while others are relatively undeformed and exhibit only a weak foliation. Garnaut (1995) divided the intrusive rocks into four broad groups: diorite and granodiorite, dolerite, amphibolite, and potassium-rich dolerite. In addition, strained (Inningarra) granite has been identified at Bunkers Hill, and the whole sequence has been intruded by The Granites Granite. The Innangarra Granite has been dated by Smith (2001) at 1,815±4 Ma, and The Granites Granite was dated by Cooper and Ding (1997) at 1,796±1 Ma.

Footwall sequence (FWS)

The FWS, whose base is invariably obscured by granitic intrusions, is characterized by intercalated pelitic and psammitic metasedimentary rocks (biotite–quartz schist, biotite–andalusite schist, biotite–almandine schist, and biotite–cordierite schist), with less common ferromagnesian amphibole-bearing lithologies (hornblende schist, amphibole schist, and magnetite–hornblende–biotite schist) that are locally mineralized (see below). The FWS is generally more than 120 m thick (Mayer 1990; Scrimgeour and Sandiford 1993), and, unlike the HWS, essentially non-graphitic. The sequence also contains thin recrystallized chert bands, which are usually 2–5 cm thick. Evidence of original sedimentary features recognizable within the FWS includes metamorphosed graded bedding, rare cross-beds, and ripple marks.

Main host unit (MHU)

The MHU hosts the majority of the gold mineralization at The Granites and is separated from both the FWS and HWS by shear discontinuities. The thickness of the MHU varies from 5–35 m over the 9-km total strike length, with maximum thickness occurring at East Bullakitchie. Mayer (1990) has previously described the MHU as being a mixed facies metamorphosed banded iron formation (BIF), where silicate and silicate-sulfide facies predominate. The MHU is thin to finely laminated and is characterized by amphibole-rich schists with lesser garnet–cummingtonite±biotite schist. Like the FWS, the MHU is graphite-free, but is more intensely deformed. The MHU is also distinguished from the FWS by the absence of andalusite, gedrite, and cordierite, and from the HWS by the absence of andalusite, cordierite, and graphite.

Hanging wall sequence (HWS)

The HWS is dominated by thin- to medium-banded pelitic schists, which grade upward into more psammitic schists. The schists show variations along and across strike. The HWS is more than 150 m thick (Mayer 1990) and can be distinguished from the FWS and MHU by the presence of accessory graphite in most rock types (excepting minor biotite–almandine garnet schist). The HWS is less competent overall than the FWS and MHU. Rock types in the HWS include biotite–quartz schist, biotite–andalusite schist, biotite–cordierite schist, graphite–quartz schist, and intensely sheared thin bands of fine-grained pyrite-rich graphitic schist (Scott 1993).

Bands of metamorphosed iron-rich metasedimentary rocks within the HWS constitute the hanging wall host unit (HWHU). These metamorphosed iron-rich metasedimentary rocks are made up of hornblende–almandine garnet–quartz schists, with or without magnetite and minor graphite. The HWHU is well laminated to thinly banded and contains intercalated chert bands.

Structure of the mine area

The structural evolution of The Granites goldfield is characterized by multiple overprinting phases of deformation. Five deformation events ($D_{1–5}$) have been identified, of which D_1 and D_3 are the most significant, with D_3 being the last major deformation event.

Intense layer parallel shearing during D_1 produced a mylonitic foliation (S_m), an elongation lineation (L_1), and boudinaged early quartz veins. Shear discontinuities formed at the MHU–FWS (Fig. 2a) and MHU–HWS (Fig. 2b) boundaries during D_1. Minor remnants of D_1 can still be identified (i.e., elongation lineation and boudins), but remaining evidence is rare due to subsequent multiple overprinting. The layer parallel shearing was not uniform in intensity across the whole sequence. The FWS acted relatively competently, while in the HWS, the graphitic schist was dismembered into highly sheared portions. The MHU was incompetent, and thus, highly sheared. This caused shear discontinuities to form along its margins, and reflects the preferred accommodation of strain in the less competent layers by layer-parallel simple shear (Treagus 1988). Early veins are boudinaged parallel to the elongation lineation (75–90° to the west), and the mylonitic foliation wraps around competent vein boudins (Fig. 2c). No D_1 folds were recognized at The Granites; however, Ding and Giles (1993) reported the presence of D_1 minor recumbent, tight to isoclinal, intrafolial folds and sheath folds within the Tanami Region.

A major D_2 deformation event in the Tanami Region resulted in compression of the previously sheared sub-horizontal layers, to produce tight upright, shallowly plunging, north–east trending isoclinal F_2 folds (Ding and Giles 1993), which caused all preexisting layering and foliation to be reoriented from sub-horizontal to sub-vertical. The Granites gold mine lies on the northwestern limb of one such major F_2 fold (P. Ding, personal communication 1992). The presence of a small isoclinal F_2 fold with a shallow plunging hinge was reported in the East Bullakitchie open pit mine (P. Ding, personal communication 1992), which showed an L_1 lineation wrapping around the hinge of the fold. Within the hinge zone of the F_2 fold, it was noted that the mylonitic foliation (S_m) had been crenulated by an intense schistosity (S_2). This was the only reported evidence for D_2 at The Granites and was subsequently destroyed during mining.

The D_3 deformation event was the last intense and pervasive event to affect the region. This event produced tight to isoclinal folds (F_3), an intense penetrative schistosity (S_3) and the reactivation of preexisting structures. Peak metamorphic temperatures were attained towards the end of, or just after, D_3 as gedrite, which is part of the peak metamorphic assemblage in semi-pelitic rocks (Scrimgeour and Sandiford 1993) is randomly oriented.

The F_3 folds (Fig. 2d) are tight to isoclinal and plunge moderately to steeply to the west. The folds are characterized by long subparallel limbs with small narrow hinge

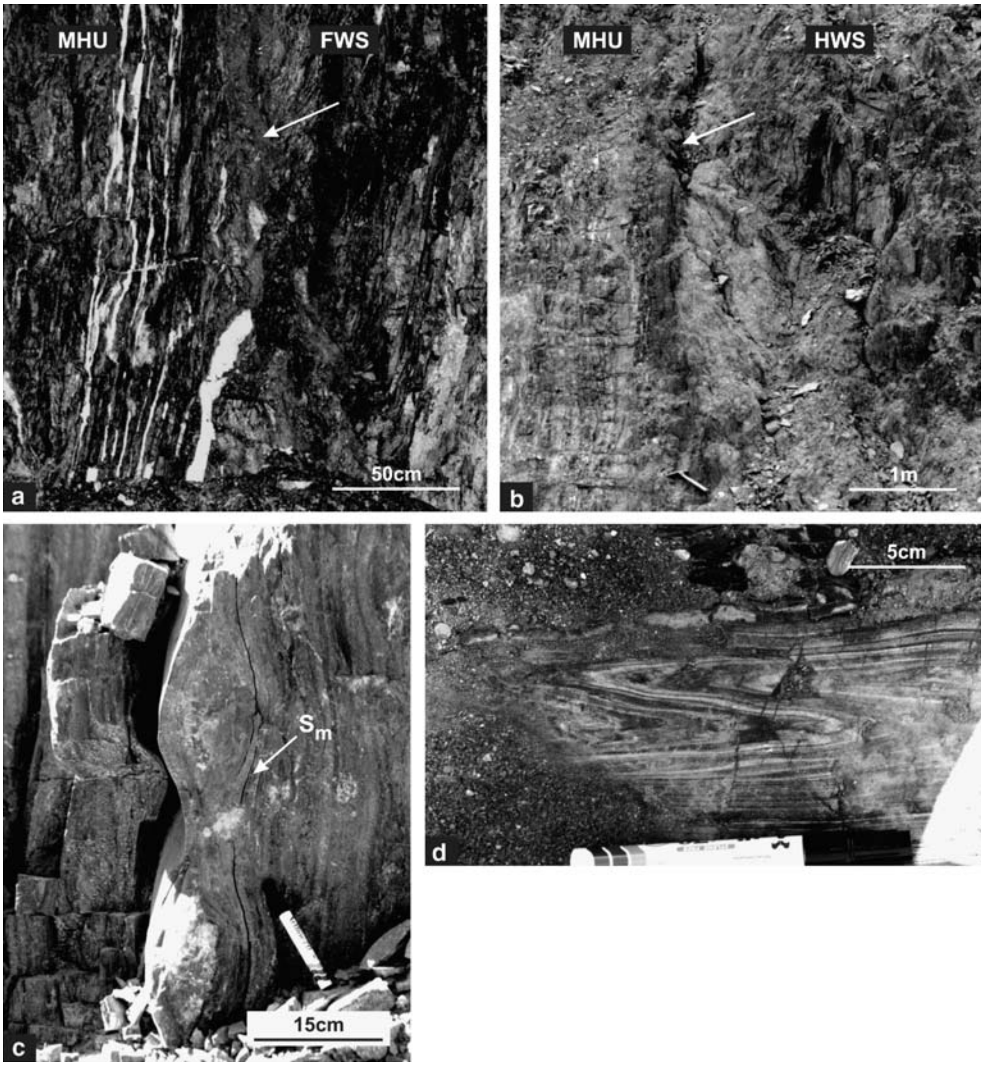

Fig. 2 **a** The FWS–MHU shear discontinuity (*arrow*) on 5 Level Cross Cut underground at East Bullakitchie, looking east; **b** The MHU–HWS shear discontinuity (*arrow*) on the western pit wall in the West Bullakitchie open cut; **c** Boudinaged quartz vein wrapped by mylonitic foliation (S_m) in the FWS at Shoe, looking east; **d** F_3 fold in the HWS at West Shoe

zones. Discrete F_3 folds are found mainly within the less competent pelitic schists, and are predominantly class 2 similar-style folds according to the Ramsay (1967) fold classification. A few F_3 folds were formed within more competent chert and quartz veins, and these are class 1c flattened parallel folds, with some rare examples of class 3 folds (Ramsay 1967). F_3 fold development is common within the HWS, and to a lesser extent in the MHU, and on the MHU–HWS contact on the pit floor at West Bullakitchie (Fig. 3). Although no recognizable F_3 folds were found within the FWS, changing cleavage vergence relationships (Bell 1981) and associated younging directions not only indicate the presence of F_3 folds, but also the presence of an earlier folding phase. The penetrative schistosity (S_3) produced as a result of D_3 is the dominant foliation observed at The Granites.

The D_4 deformation event produced a reactivation of the shear discontinuities, intense shearing in the HWS and F_4 folds with an accompanying axial planar cleavage (S_4). Towards the end of D_4, conjugate reverse faults formed, with shallow to steeply dipping planes to the north and south that offset the MHU at Shoe by 5 m. The F_4 folds are asymmetric open to close folds, with a typical geniculate (knee shaped) appearance (Fig. 4) and steep to almost

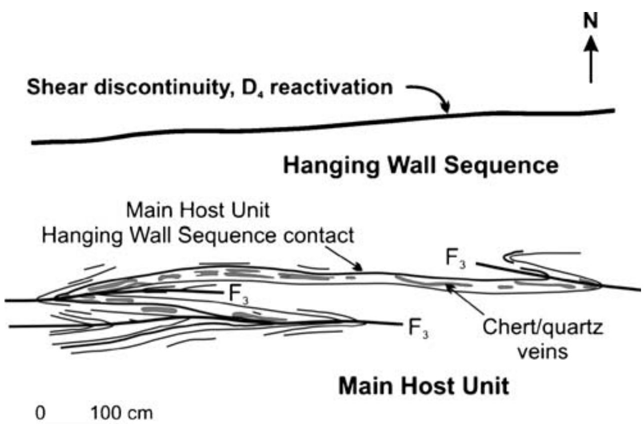

Fig. 3 Folded (F_3) contact between the MHU and HWS in West Bullakitchie open cut. The D_4 shear reactivation is also indicated 1–2 m into the HWS

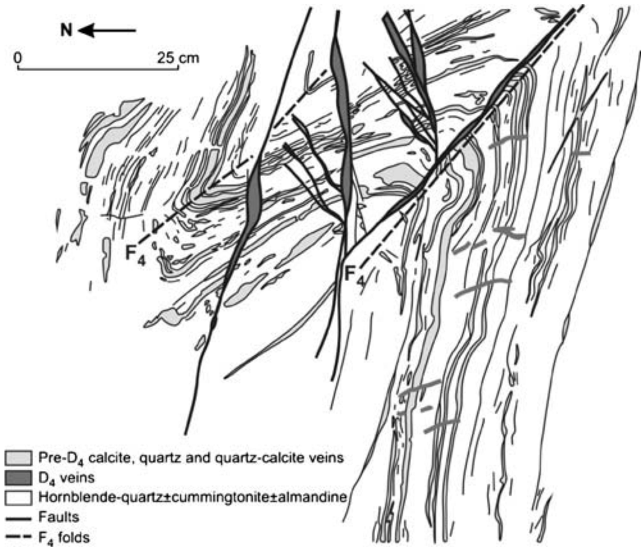

Fig. 4 F_4 folds from the MHU on 10 Level Lower Drive West, East Bullakitchie

vertical plunges to the west and northwest. F_4 folds are evident in the MHU, especially underground at East Bullakitchie where they have folded D_3 calcite veins, and within the HWS. No F_4 folds were identified within the FWS, indicating that the FWS was affected by D_4 shearing only. The resultant S_4 cleavage is only found within the fold noses of F_4 folds as an axial planar cleavage.

Reactivation of the shear discontinuities during D_4 resulted in transcurrent shearing of the sequence at The Granites. The FWS–MHU shear discontinuity appears to have been active throughout D_4 because no F_4 folds were found within the FWS. The shearing exploited earlier (D_1) shear planes, where D_4 sub-horizontal slip lineations (L_s) strongly overprinted sub-vertical D_1 slip lineations. At West Bullakitchie, the shear discontinuity between the MHU–HWS was not reactivated during D_4. F_3 folds had folded this boundary during D_3, and as a result, the shear discontinuity reactivation at this locality migrated 1–2 m into the HWS (Fig. 3). However, only 100 m to the west, in the pit face, the shear discontinuity was also reactivated along the MHU–HWS contact. This indicates that while F_3 folds have affected this contact, it is a localized phenomenon and not widespread at The Granites.

The final deformation event, D_5, was not as intense as previous events. It produced gentle to open, large scale F_5 folds with north–northeast to south–southwest axial traces. This minor folding resulted in the present orientation of The Granites host sequence. Late brittle reverse faults formed towards the end of D_5.

The structural history of The Granites gold mine outlined above correlates reasonably well with that described regionally by Ding and Giles (1993) and locally by Scott (1993) and has some correlation with the regional interpretation by Vandenberg et al. (2001). There is a close correlation between the present study and Ding and Giles (1993) for the first three deformation events. The regional D_4 of Ding and Giles (1993) has not been recognized at The Granites during this study, so that their D_5 event correlates with our D_4. Scott (1993) proposed a progressive three-phase deformation sequence that correlates with our D_2, D_3, and D_4. The more recent regional interpretation of Vandenberg et al. (2001) does not recognize our D_1 and D_2. D_1 and D_2 of Vandenberg et al. (2001) correlate with our D_3 and D_4. The last four events of Vandenberg et al. (2001) are not correlated with events presented here; however, the description of some of the reverse faulting in their later events appears to be similar to the reverse faulting identified in our D_4 and D_5.

Ore lodes

At The Granites, most ore lodes are hosted by amphibole-rich schist of the MHU, although at East Bullakitchie, two ore lodes (footwall and G lodes) are hosted by a 3- to 5-m thick interval of cummingtonite–gedrite schist in the FWS. Gold is hosted both by veins and by sulfide-rich amphibole-bearing schist. The MHU has been subdivided into A lode, B lode, and C lode, with two barren units [the MAC (massive almandine–cummingtonite schist) and Biotite Marker] of garnet–cummingtonite, and/or biotite-bearing schist between the lodes. The lodes consist of hornblende± cummingtonite schist and cummingtonite–almandine garnet schist, with accompanying pyrrhotite, arsenopyrite, and minor pyrite. Gold grades correlate both with vein abundance and sulfide content: A lode contains the highest abundance of sulfides and the highest vein density, and consequently, has the highest gold grade.

Vein geometry and mineralogy

Four vein types are recognized at The Granites according to their mineralogy: quartz, quartz-carbonate, calcite, and calc-silicate. Although most veins are unzoned, the calc-silicate veins commonly contain an inner clinozoisite–quartz zone and an outer diopside–calcite zone. Quartz veins are the dominant type, except at East Bullakitchie where an abundance of calcite veins may be a result of remobilization from localized carbonate facies BIF. Quartz, quartz-carbonate, and calc-silicate veins occur in all mine units (FWS, MHU, and HWS), whereas the calcite veins are confined to the MHU. Quartz and quartz-carbonate veins are the most important vein types with regard to gold mineralization. Based on relationships to structural elements and cross-cutting relationships, two main stages of veining were recognized. Quartz and quartz-carbonate veins developed during both main stages of veining, whereas calc-silicate

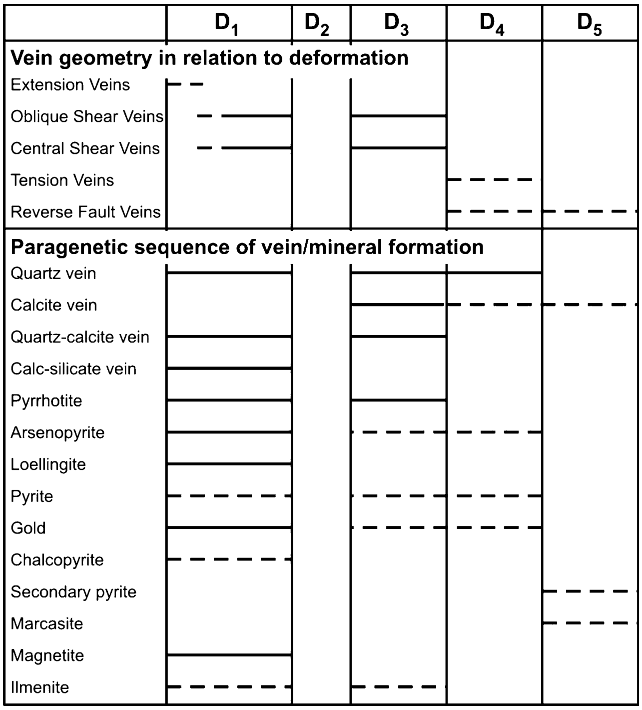

Fig. 5 Vein geometries related to the deformational sequence and the paragenetic sequence for the veins, sulphides, arsenides, oxides, and gold relative to the deformational sequence

veins developed only during the first and calcite veins developed mostly during the second period. Minor quartz and calcite veins postdated these main periods (Fig. 5).

Stage one veins

All early veins contain gold, and hence, this is the most important vein generation in the context of mineralization at The Granites. These veins, which are interpreted as both extensional and shear (fault-fill) veins, are tightly folded by ptygmatic folds formed during the development of the S_1 mylonitic fabric (Fig. 6a), are folded by both F_3 (Fig. 6b) and F_4 (Fig. 4) folds, are extensively boudinaged (Figs. 2c and 6c), and are cut by subsequent vein generations. The extensional veins, although containing gold, are not as numerous as the shear veins, which host the majority of the vein-associated gold. The early veins are observed parallel and slightly oblique to the main (S_3) layering and schistosity. Early D_1 quartz veins formed during the onset of shearing as extension veins and are cut by subsequent syn-D_1 quartz shear veins. As these veins are overprinted by all structural elements at The Granites, they are interpreted to have formed during D_1 (Fig. 5).

Stage two veins

The second major vein generation consists of quartz, quartz-carbonate, and calcite veins (Fig. 5). The calcite veins and a small proportion of quartz and quartz-carbonate veins have been folded by F_4, and rarely, F_3 folds. Most quartz and quartz-carbonate veins of this generation, however, have been folded by F_3 folds (Fig. 3), although they cross-cut stage one veins. These early stage two quartz and quartz-carbonate veins contain gold, and some gold has also been observed in late stage two calcite veins (T. Mayer, personal communication 1992). The quartz and quartz carbonate veins are interpreted to have formed early during D_3 as they cut stage one veins but are folded by F_3 folds, whereas the calcite veins are interpreted to have formed during the waning stages of D_3 as they are rarely folded by F_3 folds.

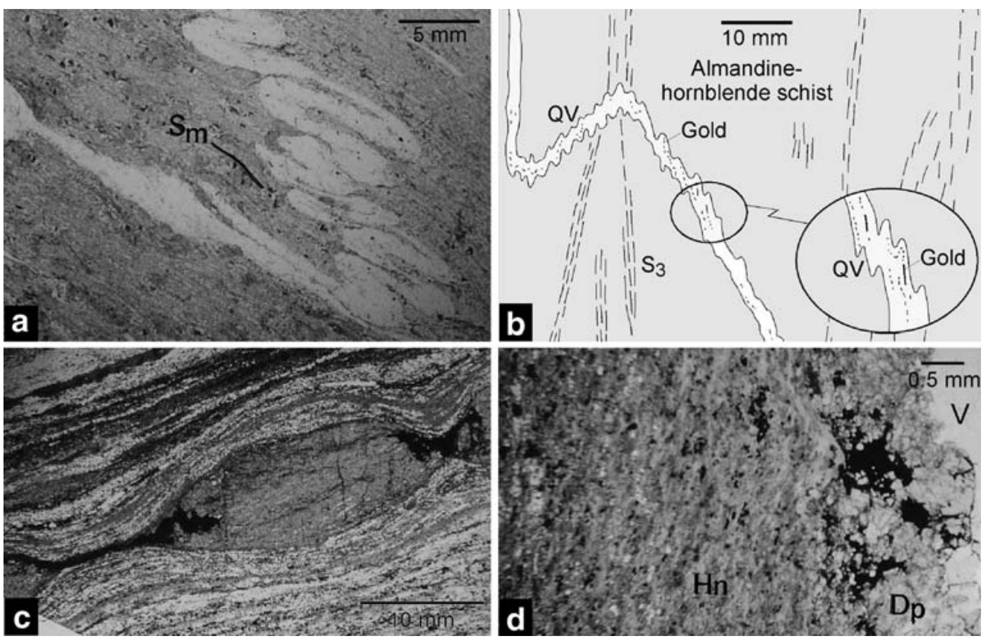

Fig. 6 **a** Ptygmatically folded, auriferous stage one vein with mylonitic (S_1/S_m) fabric defined by biotite. **b** Sketch of folded, auriferous, cherty vein (QV) that is folded and crenulated by F_3/S_3. Modified after Mayer (1990) to reflect current structural terminology. **c** Boudinaged stage one calc-silicate vein wrapped by S_3 defined by biotite and chlorite. Note sulfide minerals in boudin necks. **d** Zoned alteration assemblage adjacent to quartz-carbonate. Mineralogy grades from diopside-rich next to vein to hornblende-rich. Fabric defined by hornblende is S_3

The presence of “centipede veins” (Hodgson 1989a) in stage two suggests that this generation involved a minor extensional phase that occurred as a result of slippage along shear planes. At The Granites, the dominant shear veins (central or oblique) are connected by thin extension veinlets of the same generation.

Late veins

Late stage veins, which cross-cut both of the early vein stages and F_3 and F_4 (Fig. 4) are filled by quartz and calcite. These veins are interpreted to have formed mostly during D_4 (Fig. 5), partly in response to the development of tension cracks in the hinges and limbs of the F_4 folds (Fig. 4). Late D_4 reverse faults are also commonly found to contain quartz and/or calcite infill, along with associated chlorite and pyrite. The fault-fill veins associated with the reverse faults commonly occur as a conjugate set, with the sinistral faults and veins being more prominent and better developed. Some late reverse faults that formed during D_5 contain minor calcite (± chlorite and pyrite) veins (Fig. 5).

Wall rock alteration associated with veins

Narrow (to 1 cm), zones of wall rock alteration are found adjacent to many veins at The Granites. Although wall rock alteration adjacent to quartz veins is uncommon, when present, it is dominated by hornblende, with minor cummingtonite and epidote. Wall rock alteration adjacent to calcite and quartz-carbonate veins is relatively common.

Calcite veins are associated with zoned, calcium-rich alteration assemblages which pass from a diopside–clinozoisite-rich zone adjacent to the vein to a hornblende-rich zone (Fig. 6d), and then, into a cummingtonite-rich zone. A small proportion of calcite veins lack the inner diopside–clinozoisite zone. Alteration associated with the quartz-carbonate veins is very similar, the main difference being that the diopside and clinozoisite form part of the vein assemblage, rather a proximal alteration zone. Calc-silicate veins commonly exhibit an alteration selvage which grades outwards from hornblende-rich to a cummingtonite–hornblende zone. With the exception of quartz-only veins, most veins are characterized by an overall wall rock alteration zonation of diopside–clinozoisite → hornblende → cummingtonite, with the diopside–clinozoisite assemblage within the veins in quartz-carbonate and calc-silicate veins. As alteration minerals such as hornblende (Fig. 6d) and cummingtonite are strongly aligned into the S_3 fabric, wall rock alteration associated with the veins developed during or before D_3, consistent with the inferred timing of the veins. This relationship and metamorphic textures (Scrimgeour and Sandiford 1993) that indicate peak metamorphic conditions during D_3 suggest that mineralization in The Granites goldfield predated or accompanied peak metamorphism.

In a more detailed study of vein alteration assemblages from the footwall lode at East Bullakitchie, Scrimgeour and Sandiford (1993) observed that the inner diopside–clinozoisite zone also contains garnet, with accessory to minor hornblende, quartz, feldspar, sphene, rutile, allanite, prehnite, apatite, and scheelite. The hornblende-rich zone also contains plagioclase, epidote, and quartz, with accessory apatite, sphene, and ilmenite, with sphene dominating the inner, and ilmenite, the outer part of this zone. In the outer cummingtonite-rich zone, quartz and plagioclase are also present, with accessory ilmenite and local gedrite on the outermost margin (Scrimgeour and Sandiford 1993).

This zonation led Scrimgeour and Sandiford (1993) to infer that metasomatism associated with veining and gold introduction involved the removal of K and addition of Ca as biotite in the wall rock broke down to form cummingtonite, which in turn, was altered to hornblende, which was converted to the assemblage diopside–clinozoisite±garnet adjacent to or within the vein. In addition to these changes, the metasomatic reactions appear to involve oxidation of the wall rocks as indicated by zonation in Ti-bearing minerals [sphene (in vein) → ilmenite → biotite (in wall rock)] and the increased abundance of Fe^{3+}-bearing minerals such as clinozoisite within and immediately adjacent to the veins. Scrimgeour and Sandiford (1993) described the local presence of corroded, apparently pre-metasomatic, garnets within the outer part of the alteration selvages, suggesting that the metasomatism occurred at high temperatures. A more detailed account of the alteration assemblages and the metasomatic reactions that formed them may be found in Scrimgeour and Sandiford (1993).

Sulfide–arsenide-bearing ores

In addition to the veins described above, sulfides and arsenide minerals are also concentrated within ore lodes in The Granites goldfield, although their distribution is independent of vein density. The sulfide–arsenide content of the footwall lode, G lode and HWHU ore bodies is higher than in the surrounding FWS and HWS schists but lower than in the MHU. The assemblage is dominated by pyrrhotite, arsenopyrite and loellingite, with lesser pyrite, minor chalcopyrite, rare marcasite, and very rare galena. Magnetite and ilmenite have a combined abundance similar to that of pyrrhotite, while rare hematite is also present. Microscopic gold is present as inclusions within arsenopyrite and loellingite, and rarely observed in pyrrhotite and chalcopyrite. Arsenopyrite, although not the most abundant sulfide, is the most important in terms of its association with gold. The sulfide–arsenide assemblage preferentially occurs in more amphibole-rich layers within the MHU.

The sulfide–arsenide mineralization occurs parallel to layering and schistosity, suggesting formation was contemporaneous with, or earlier than, the deformation that produced that schistosity. The sulfide–arsenide assemblage also preferentially occurs in the more amphibole-rich layers within the MHU, suggesting either syn-sedimentary deposition or that these layers acted as chemical traps as fluids migrated through the metasedimentary pile during deformation.

Structural relationships indicate two generations of sulfide–arsenide growth (Fig. 5). Evidence for an early generation includes development of arsenopyrite and pyrrhotite along S_1–S_m preserved within a boudin that formed during D_3 (Fig. 7a). In this example, the fabric developed by the sulfide minerals does not extend outside of the boudin, implying at minimum that the sulfides were emplaced before D_3. Additional evidence for early stage sulfide mineralization includes the folding of a sulfide-rich band by a F_3 fold (Fig. 7c and d), the wrapping of D_1 boudins by pyrrhotite, and systematic differences in sulfur isotope compositions between the two inferred sulfide–arsenide generations (see below). These observations strongly imply an early phase of mineralization before D_3 and probably associated with D_1. Other minerals associated with this first generation include loellingite and minor pyrite and chalcopyrite (Fig. 5).

At the macro- and microscales, pyrrhotite occurs either as laminae parallel to S_1–S_m, or as inclusions within arsenopyrite. Arsenopyrite, like pyrrhotite, is also layer parallel. Early stage arsenopyrite is intensely stretched parallel to the S_1–S_1 foliation (Fig. 7a) and contains inclusions and intergrowths of loellingite (Fig.7b), pyrrhotite, chalcopyrite, magnetite, gold, and pyrite. The pyrite commonly has replaced pyrrhotite.

Second generation pyrrhotite, arsenopyrite, and pyrite are interpreted to have formed syn- to post-D_3 (Fig. 5). Pyrrhotite and pyrite occur as small streaks parallel to the S_3 schistosity, indicating a D_3 origin. Where syn-D_1 pyrrhotite is folded by F_3 folds (Fig. 7c and d), syn- to post-D_3 pyrrhotite can be seen parallel to the S_3 schistosity within F_3 fold hinges. The latter pyrrhotite is interpreted to have formed as a result of remobilization of first generation

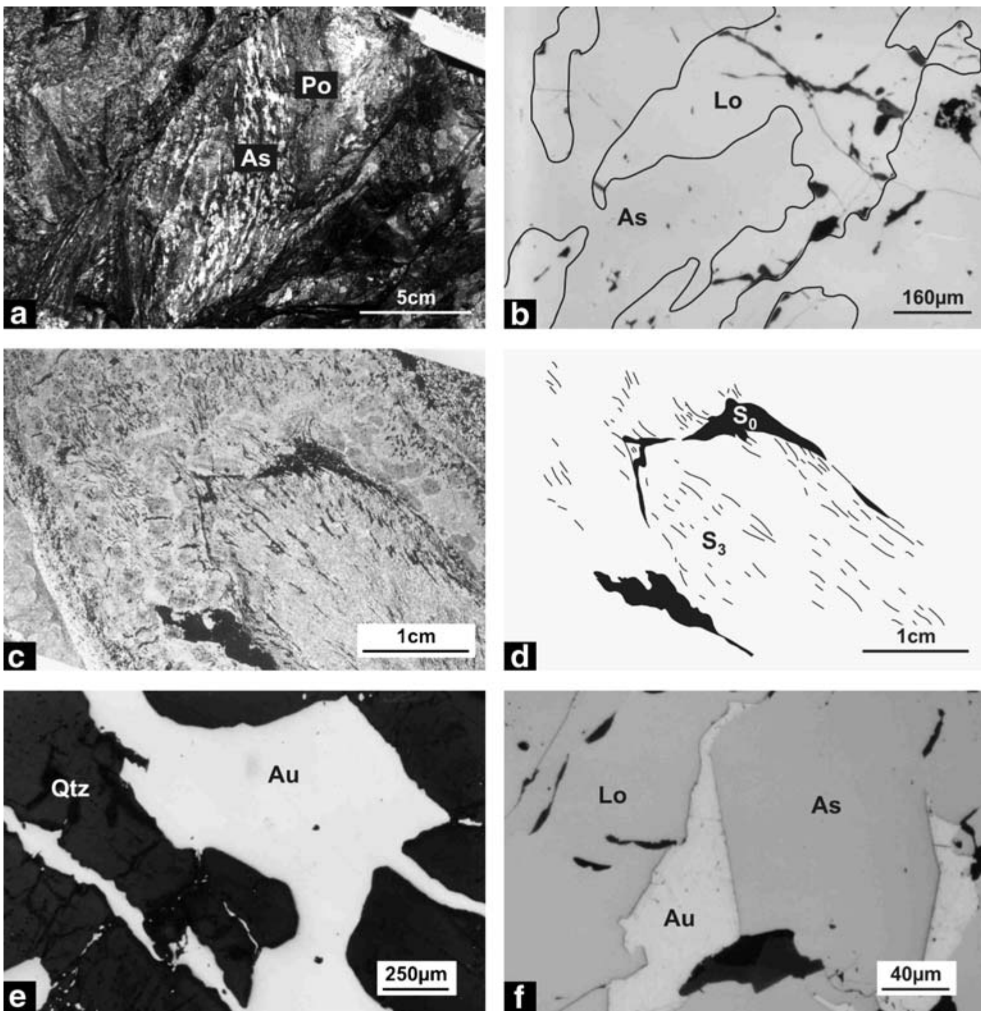

Fig. 7 **a** Arsenopyrite and pyrrhotite stretched parallel to the early foliation (S_m) and boudins within the MHU, Shoe Drive East (1259RL), looking east; **b** Loellingite coexisting with arsenopyrite, GQD147 (109.85 m), Quorn deposit, reflected light; **c** F_3 fold with layer parallel first generation pyrrhotite (S_0=S_m) and second generation pyrrhotite parallel to the schistosity (S_3), GBD205 (171.90 m), Bullakitchie deposit; **d** Sketch of Fig. 8c; **e** Gold within D_1 quartz vein, 8 Level G Lode, East Bullakitchie, reflected light; **f** Gold with arsenopyrite and loellingite, Shoe underground, reflected light. As Arsenopyrite, Au gold, Lo loellingite, Po pyrrhotite, Qtz D_1 quartz vein

pyrrhotite. Inclusion free, second-generation arsenopyrite, pyrrhotite, and pyrite are also found trapped within D_4 quartz veins, indicating D_4 remobilization. A syn- to post-D_3 timing for this generation is proposed to account for the D_3 to D_4 overlap. The minerals of this generation make up only a minor amount of the overall sulfide–arsenide content, which is interpreted to have formed mainly during D_1.

Gold commonly is associated with early, syn-D_1 sulfides and arsenides, indicating deposition of gold at the same time as that within D_1 quartz (Fig. 7e), quartz-carbonate, and calc-silicate veins. Microscopic gold is common within syn-D_1 arsenopyrite and loellingite (Fig. 7f) but was not observed in syn- to post-D_3 arsenopyrite. The deformation of sulfides during D_3 may have remobilized gold that is now found in D_3 veins. Larocque et al. (1993) suggested that metamorphic remobilization is important in releasing and locally concentrating refractory gold from sulfides. The degree of remobilization, and thus, release of gold will be related to the degree of metamorphic recrystallization. The limited amount of sulfide recrystallization and remobilization at The Granites could explain the relatively low concentrations of gold in D_3 quartz and quartz-carbonate veins with respect to their D_1 equivalents.

Constraints on the conditions of metamorphic recrystallization of the ores

Textural relationships documented previously suggest that most, if not all, of the ore textures observed in The Granites goldfield have been affected by metamorphic recrystallization after ore deposition. Although this complicates the interpretation of fluid inclusion microthermometry and stable isotope data, these data can provide insight into conditions of metamorphism and to a limited extent, the sources of ore constituents.

Constraints from fluid inclusions

Although investigations of fluid inclusions within polydeformed and metamorphosed ore deposits provide insights into fluid evolution accompanying metamorphism, use of these data to constrain the primary conditions of metamorphism potentially can be difficult. Investigations on polydeformed and metamorphosed ore deposits commonly use the so-called “primary” fluid inclusions to interpret the microthermometric data, but misinterpretation of the timing of (i.e., primary vs secondary) fluid inclusions has direct ramifications for the interpretation of the fluid evolution for an ore deposit (Giles and Marshall 1994a, 1995). Strict adherence to Roedder’s (1984) timing criteria can lead to misidentification of the fluid inclusion type, as secondary fluid inclusions can develop negative crystal morphologies, high degrees of healing may obscure initial microfractures, and inclusions may migrate way from microfracture planes (Giles and Marshall 1994a,b, 1995). Furthermore, genuine primary fluid inclusions related to the early history of metamorphosed veins are infrequently encountered because of the problems of recrystallization and decrepitation (Barker 1990).

To assess these issues, quartz was selected for fluid inclusion analysis from D_1, D_3, and D_4 veins from the MHU, the footwall lode, and G lode. D_5 veins were not sampled, as they consist only of calcite. The fluid inclusions observed at room temperature were: (1) decrepitated (Fig. 8a) and/or leaked fluid inclusions (Fig. 8b), and (2) fluid inclusions within microfractures or inclusion trains having consistent vapor to liquid ratios. Although no definitive primary fluid inclusions were identified, secondary fluid inclusions were abundant within all quartz vein generations, either along or in close proximity to healed microfractures.

Decrepitated and/or leaked fluid inclusions occur within all quartz vein generations. Leaked fluid inclusions exhibit a variety of forms, including common irregular fluid inclusions that show evidence of necking down (Fig. 8b). Some leaked fluid inclusions display a characteristic hook-like shape (as described by Vityk and Bodnar 1995), whereas in rare instances, fluid inclusions exhibit an annular morphology (Fig. 8c). Decrepitated fluid inclusions (Fig. 8a) are generally larger than the leaked variety and are dark due to the loss of fluid during rapid, explosive decrepitation. These fluid inclusions are commonly surrounded by a halo of satellite fluid inclusions with variable vapor/liquid ratios, and satellite fluid inclusions can also be seen in some of the fracture planes emanating from decrepitated fluid inclusions.

Secondary fluid inclusions with consistent fluid/liquid ratios occur in all vein generations. These fluid inclusions all occur along healed microfractures (Fig. 8d) and are mostly liquid-rich with up to 25% vapor. The most common fluid inclusion type was two phase (liquid + vapor), although three phase fluid inclusions (liquid + vapor + solid) (Fig. 8e) and CO_2-rich fluid inclusions (Fig. 8f) were observed, the latter only in samples from the footwall and G lodes.

First-melting (eutectic) measurements of two phase inclusions ranged from −1 to −84°C (Fig. 9a), indicative of fluids with a range of compositions beyond simple H_2O–NaCl (Davis et al. 1990). The presence of these salts was confirmed by laser Raman analyses of frozen inclusions, which yield Raman peaks at ~3,438, 3,383, and ~3,510 cm^{-1} (Adams 1997) indicating the presence of NaCl, $CaCl_2$, and $MgCl_2$, respectively. Using eutectic temperatures and the criteria of Davis et al. (1990), the

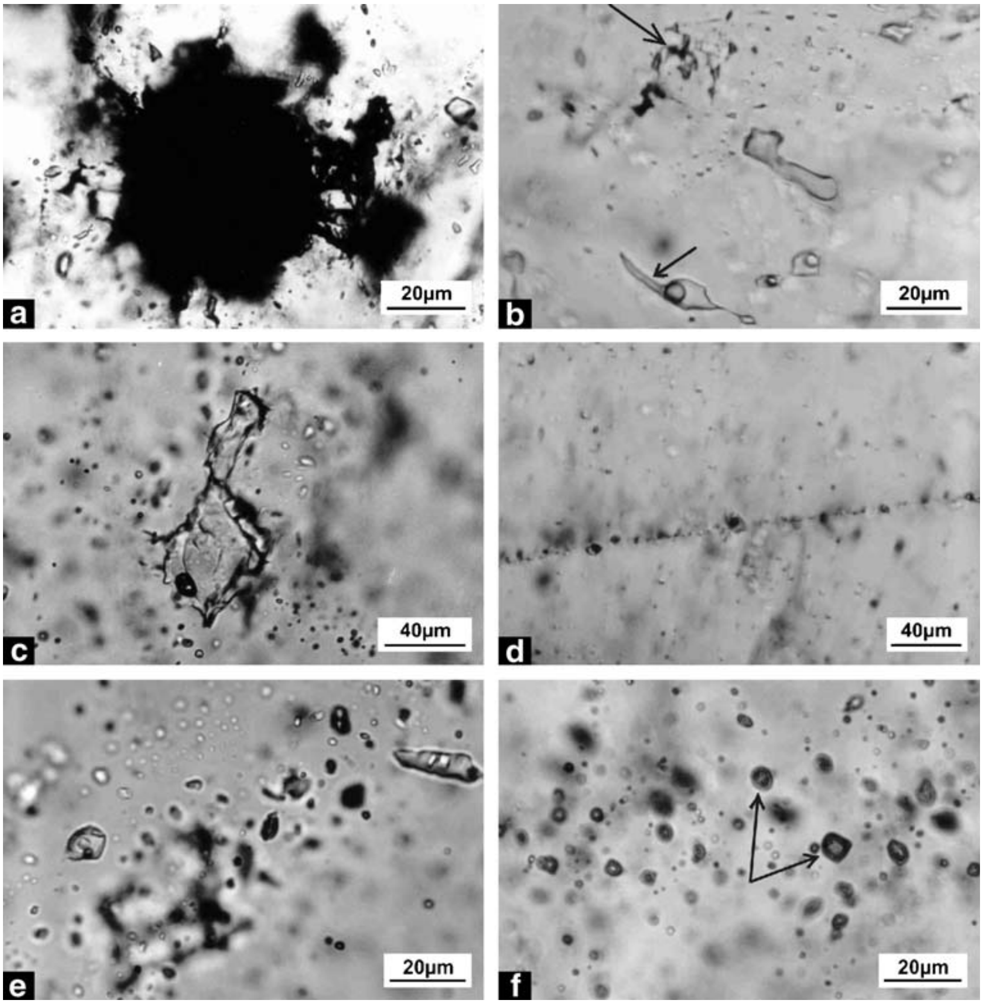

Fig. 8 **a** Decrepitated fluid inclusion (*black*), GSD196 (162.20 m), Shoe deposit; **b** Leaked fluid inclusion (*arrow*), Shoe Drive East (1268RL); **c** Fluid inclusion exhibiting rare annular morphology, GBD205 (171.90 m), Bullakitchie deposit; **d** Healed microfracture containing small secondary fluid inclusions, 4 Level Lower Lode, East Bullakitchie; **e** Fluid inclusions exhibiting solid daughter minerals with liquid and vapor, Shoe Drive East (1268RL); **f** CO_2-rich fluid inclusions (*arrows*), 12 Level Footwall Lode, East Bullakitchie

two-phase inclusions were divided into three types based on the dominant salt present, H_2O–NaCl±KCl, H_2O–$MgCl_2$±NaCl, and H_2O–$CaCl_2$±$MgCl_2$±NaCl.

Final melting temperatures ranged from −43 to 0°C (Fig. 9b), with the NaCl-rich inclusions between −21 and 0°C, the $MgCl_2$-rich inclusions between −28 to −21°C, and the $CaCl_2$-rich inclusions between −43 and −3°C, which correspond to salinities, as calculated using the equation of Potter et al. (1978), of 0–24 eq wt% NaCl (median=0.2 eq wt% NaCl), 2–28 eq wt% NaCl (median= 10 eq wt% NaCl) and 5–40 eq wt% NaCl (median=24 eq wt % NaCl), respectively. Final melting temperatures of CO_2-rich vapor ranged between −57.1 to −55.8°C, indicating nearly pure CO_2, a result confirmed by laser Raman analyses (Adams 1997).

Measurements of homogenization temperatures ranged from 100 to 420°C for aqueous fluid inclusions, with no systematic relationship with the dominant salt in the fluid inclusion (Fig. 9c). The large range in homogenization temperatures may reflect necking and other post-entrapment changes, some of which may have occurred as the result of metamorphic recrystallization. The carbonic phases of CO_2-bearing fluid inclusions, which were found only within the footwall and G lodes, homogenized at 25 to 31°C.

As part of a larger district-scale fluid inclusion study, Mernagh and Wygralak (2006) found a larger abundance of CO_2-rich inclusions in The Granites samples and also reported the presence of nitrogen and methane. The presence of carbonic inclusions, as reported in both studies, is consistent with studies on other Proterozoic gold deposits, which indicate that CO_2 is a common component in the mineralizing fluids (e.g., Fedorowich et al. 1991; Ibrahim and Kyser 1991; Ettner et al. 1994).

Structural relationships suggest that the gold-bearing veins and mineral assemblages have been significantly affected by post-ore metamorphic recrystallization, which would also have affected ore-related fluid inclusions. It is likely that the fluid inclusions observed in this study record mostly post-ore fluids, and caution should be exercised in interpreting the fluid inclusion data from metamorphosed lode-gold deposits.

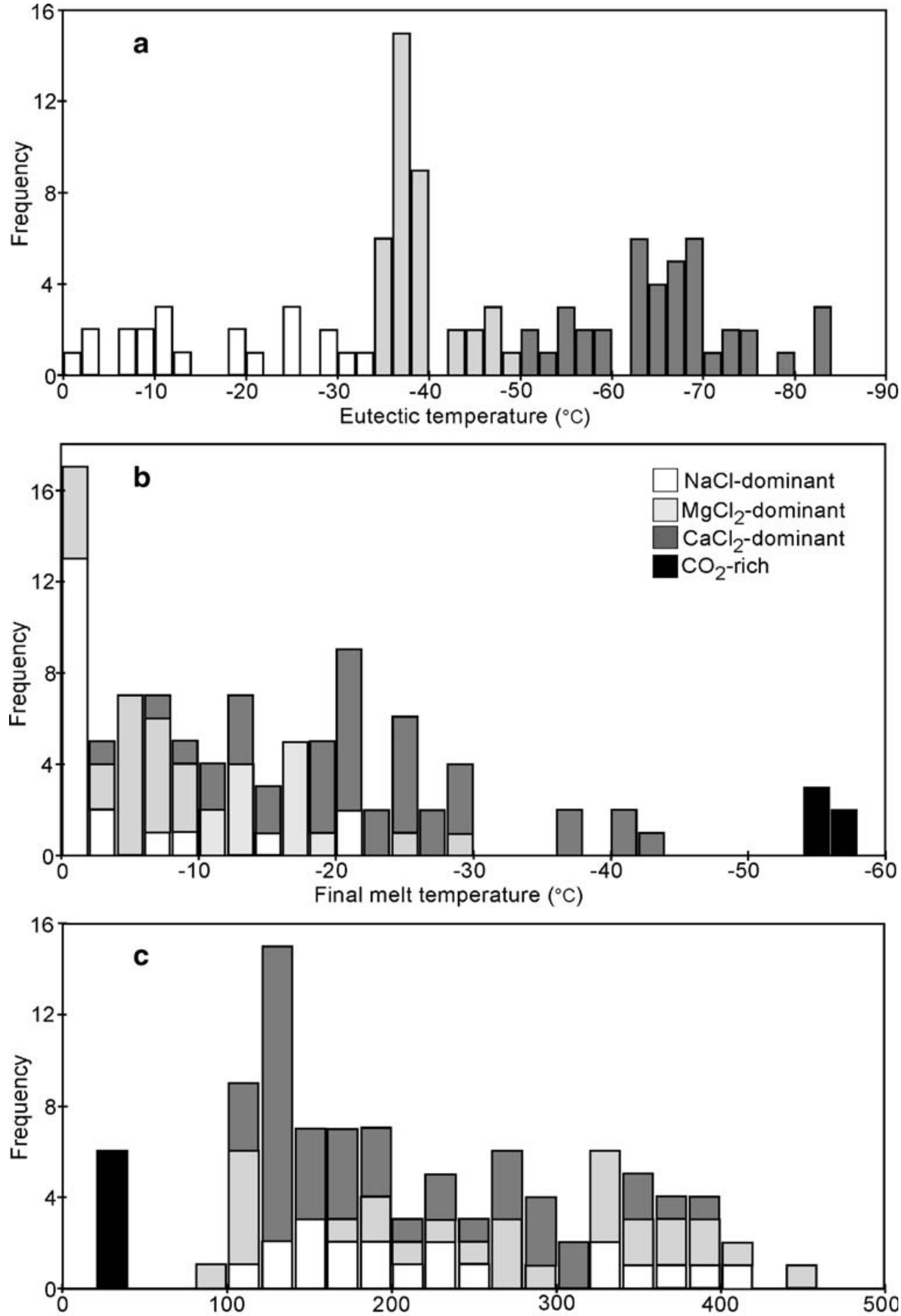

Fig. 9 Histograms summarizing fluid inclusion microthermometric data. **a** First melting temperatures. **b** Final melting temperatures. **c** Homogenization temperatures

Sulfur isotopes

Samples for sulfur isotope analyses were selected from drill core or collected from underground mines. SO_2 was prepared from 44 pyrrhotite and 33 arsenopyrite concentrates according to the method of Robinson and Kusakabe (1975). $\delta^{34}S$ values were determined on a Micromass 602E mass spectrometer at the University of Adelaide, with a reproducibility of ±0.2‰. In addition, three samples containing both syn-D_1 and syn- to post-D_3 sulfides were selected for in situ sulfur isotope analyses of pyrrhotite, pyrite, and marcasite by laser ablation at the Scottish Universities Environmental Research Centre (SUERC), East Kilbride. SO_2 was prepared according to the method described by Kelley and Fallick (1990). $\delta^{34}S$ values were determined on a VG SIRA II mass spectrometer with a reproducibility of ±0.2‰ and corrected for mineral-dependent fractionation following Kelley and Fallick (1990).

Conventional analyses of 62 samples of syn-D_1 pyrrhotite and arsenopyrite show a range of $\delta^{34}S$ values between 4.2 and 8.6‰ (Fig 10a), whereas conventional analyses of 15 samples of syn- to post-D_3 pyrrhotite and arsenopyrite have $\delta^{34}S$ values from −2.3 to 4.0‰ (Fig. 10b). $\delta^{34}S$ values obtained by in situ laser ablation analyses are consistent with the results of the conventional analyses; syn-D_1 sulfides (three pyrrhotite and three pyrite) range from 5.4 to 8.6‰ (Fig. 10a), and syn- to post-D_3 sulfides (two pyrrhotite and one marcasite) range from 0.0 to 3.2‰ (Fig. 10b). These data support the interpretation of two distinct stages of sulfide–arsenide mineralization.

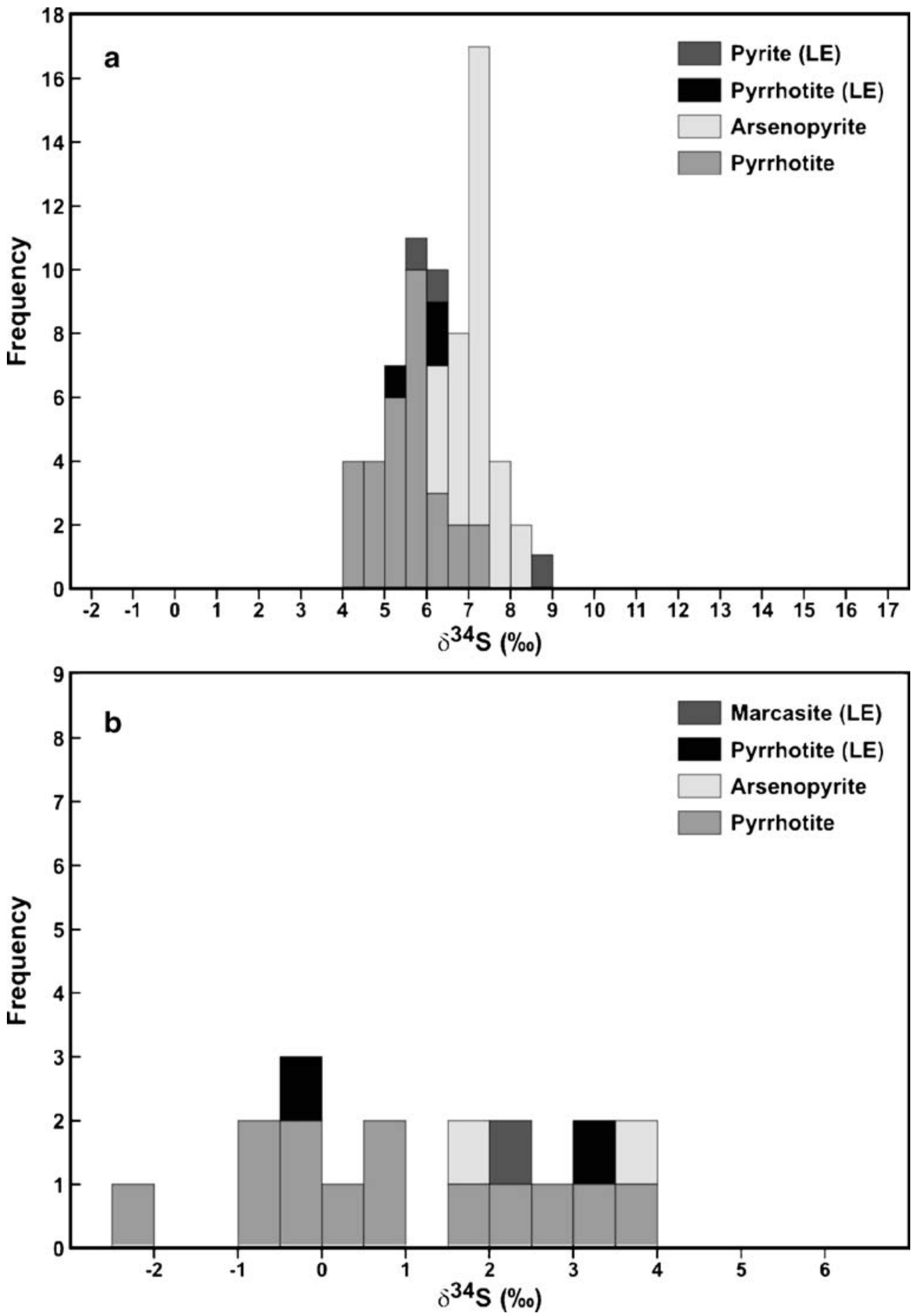

Fig. 10 $\delta^{34}S$ histograms for **a** syn-D_1 sulfides and **b** syn- to post-D_3 sulfides. LE Analyses by laser ablation

Discussion

Structural control is an important factor in the formation of many types of gold deposits. Most vein-type lode-gold deposits are hosted in brittle and brittle–ductile shear zones, and to a lesser extent, by extensional veins (Hodgson 1989a). Despite the importance of structural control, some deposits, such as The Granites, Lupin (Lhotka and Nesbitt 1989), and Homestake (Rye and Rye 1974), are also stratabound due to a strong host-rock control (e.g., BIFs).

Gold deposition at The Granites clearly occurred early in the deformational history. All D_1 quartz, quartz-carbonate, and calc-silicate veins contain gold; small (2–5 mm wide) quartz veins of this generation host the majority of the vein-related gold. Later vein generations (D_3 and D_4) contain only a small amount of gold, which can be accounted for by remobilization of preexisting gold during formation of these veins. Syn-D_1 sulfides also contain gold, while all post-D_1 sulfides are free of gold. The interpretation of an early syn-tectonic ore genesis is consistent with Scrimgeour and Sandiford (1993) and Valenta and Wall (1996) who also favor early genesis. This, however, differs with the interpretation of Vandenberg et al. (2001) and Wygralak et al. (2001) who proposed a late-tectonic age for the mineralization.

Structural controls

Like The Granites deposits, many other Archaean and Proterozoic gold deposits occur in shear zones that formed early in the deformational sequence (e.g., Starra and Trough Tank, Queensland: Davidson et al. 1989; How Mine, Zimbabwe: Harley and Charlesworth 1990; Hollinger-McIntyre gold–quartz vein system, Canada: Burrows et al. 1993). These gold deposits formed in ductile–brittle shear zones, where ductile and brittle deformation developed at different stages. The continued structural evolution of most deposits involved either folding or late brittle faulting, both of which are recognized at The Granites (e.g., shear reactivation during D_4 and reverse brittle faulting late D_4 and D_5). Ductile–brittle shear zones are characterized by the development of a strong foliation (Roberts 1988), which at The Granites is represented by the penetrative S_3 schistosity.

Shear zones create ideal structural pathways for the migration of ore forming fluids and also control the dilation of the host material to produce structural sites for vein formation. These processes characterize many lode-gold deposits worldwide (e.g., Groves et al. 1987; Kerrich 1989; Bloem et al. 1994; Robert et al. 1994), with the shear zones characterized by an anastomosing geometry, in which a network of high strain zones surround low strain rhomboids (Hodgson 1989b). At The Granites goldfield, the MHU is the most intensely sheared unit, with most veins localized in low strain pockets. The most common vein geometries are central shear veins (parallel to the C shears) and oblique shear veins (inclined to the shear zone boundaries in the same way as P shears), with extension veins relatively uncommon (Fig. 11).

Figure 12 shows the geometric relationships between structural elements and veins that could be expected during D_1 at The Granites. The extension veins, which developed first, formed at a high angle to the schistosity, and were subsequently folded, whereas shear veins formed parallel and with low angle obliquity to the schistosity (Fig. 12). This is consistent with Hodgson (1989b), who noted that in many mineralized shear zones, there is an early set of highly deformed veins, which probably formed as en-echelon extension vein arrays at the early stage of shear development. The early quartz veins at The Granites are oblique to the schistosity and layering. Subsequent shearing has rotated these veins towards parallelism with the shear direction, causing some veins to ptygmatically fold, whereas others were boudinaged as D_1 shearing continued. Deformation of these veins indicates that they were emplaced very early during the development of the shear

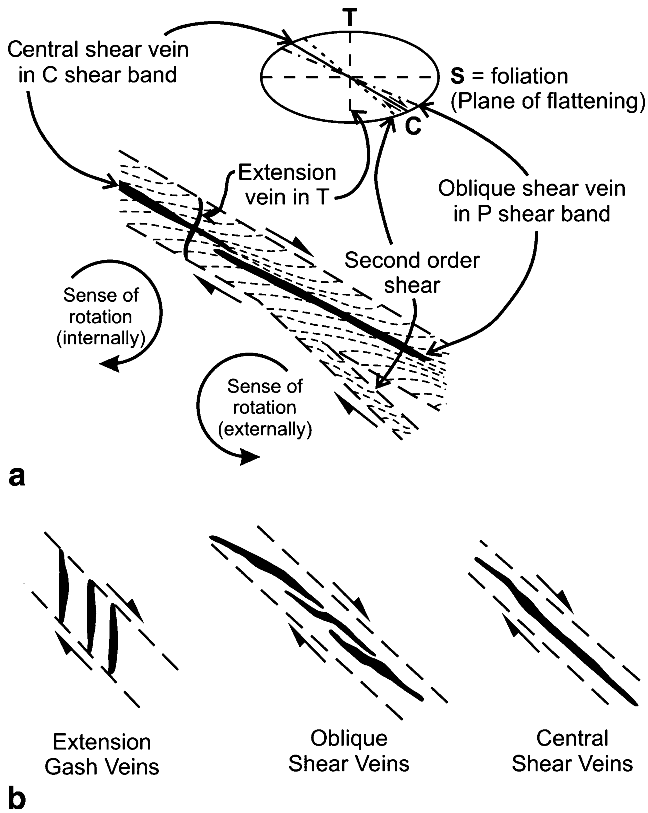

Fig. 11 **a** Structural features of shear zones and associated vein types, in relation to the strain ellipse. Modified from Hodgson (1989b); **b** Common vein geometries seen at The Granites. Modified from Hodgson (1989a)

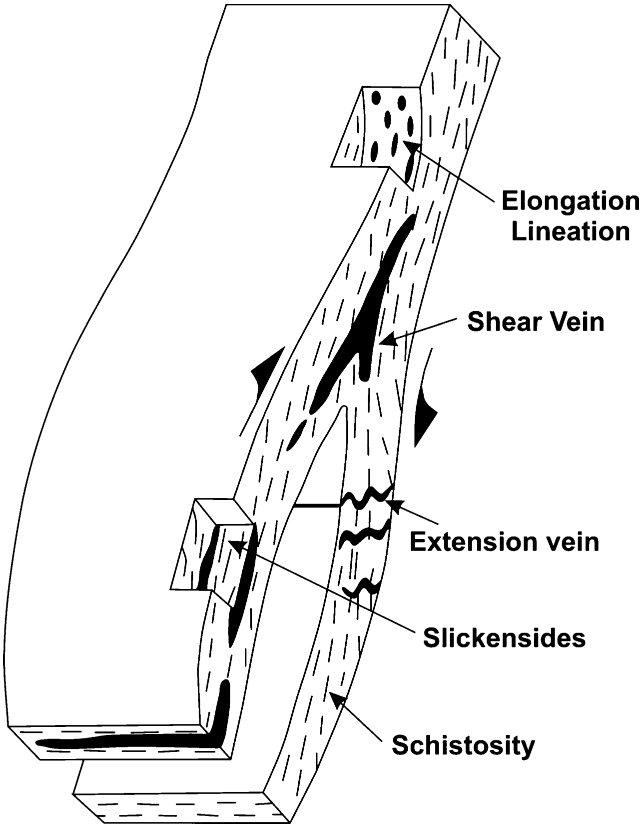

Fig. 12 Sketch showing the geometric relationships between structural elements of shear zones and related vein development. Modified from Robert et al. (1994)

zone, as was observed by Robert and Brown (1986a) at the Sigma Mine in Ontario.

Like many vein-type gold deposits in Canada (Val d'Or: Robert 1990; Robert and Brown 1986a,b; and in Ontario: Colvine et al. 1988), shear (fault-fill) veins, which include quartz, quartz-carbonate, and calc-silicate veins, are the most common D_1 vein type at The Granites. These veins have taken advantage of layer parallel shear fractures (Hodgson 1989a), thus, producing oblique and central shear veins (Fig. 11b). Shear veins are typically laminated (Robert et al. 1994), and this can be seen at The Granites where quartz-carbonate, and to a lesser extent, quartz veins are commonly separated by slivers of foliated wall rock. Hodgson (1989b) and Robert et al. (1994) reported that an entire spectrum of laminated shear veins exist, from sheeted veinlet zones (in which the proportion of wall rock is equal to, or greater than, the vein content) to ribbon-textured veins (in which the vein component dominates). The laminated and ribbon textures of the vein indicate repeated episodes of fracturing and vein emplacement. At The Granites, the wall rock slivers within the veins are as strongly foliated as the host rock surrounding the veins, indicating that the veins must have developed in an active shear zone rather than overprinted by the shear zone, as noted by Robert et al. (1994).

Chemical controls

Four phases of hydrothermal fluid activity were responsible for the four vein generations at The Granites. Sulfide deposition was related to the first two phases, with only minor sulfide deposition in the last two. Because of recrystallization and re-equilibration during each deformation period, the veins from D_1 and D_3 have apparently not preserved any primary fluid inclusions, which limits inferences about the conditions of ore formation.

Phase one: initial gold mineralization during D1

The first phase of hydrothermal fluid activity produced D_1 quartz, quartz-carbonate, and calc-silicate veins and syn-D_1 sulfides. The calcite in the veins is interpreted as having been derived from local carbonate facies BIF, whereas the quartz, sulfide minerals, and gold were derived externally. Little is known about syn-D_1 fluid conditions, apart from the fact that the sulfide assemblage (dominated by pyrrhotite–arsenopyrite–loellingite, with minor pyrite) indicates a relatively sulfur-poor fluid and that textural relationships suggest that mineralization occurred during prograde metamorphism, before peak temperatures of ~600°C. Alteration assemblages associated with gold-bearing veins suggest that the ore fluid added Ca but removed K from the wall rock. Variations in Fe- and Ti-bearing minerals also suggest that the ore fluid was more oxidized than the wall rock.

Although these conditions might be expected to favor transport of the gold by the chloride complexes rather than bisulfide complexes (Huston and Large 1989), the lack of abundant silver and base metals at The Granites suggests that transportation by a bisulfide complex is more likely. This is supported by Mikucki and Groves (1990) who postulated that the AuHS° complex may become increasingly important at high temperatures.

Precipitation of sulfides and gold took place preferentially in the iron-rich rocks of the MHU, presumably as a result of fluid–wall rock interaction. Reaction of H_2S-bearing fluids with iron-rich wall rocks with high Fe/(Fe+Mg) favors precipitation of iron-bearing sulfides (Phillips et al. 1984; Böhlke 1989). As the Fe/(Fe+Mg) ratio and total iron content of the MHU at The Granites is higher than those of FWS and HWS, and the MHU is structurally favorable, being highly sheared within two shear discontinuities, this unit was a highly effective trap for gold. As gold transport was most likely dominantly as the bisulfide complex, the precipitation of sulfide minerals would have caused gold deposition due to a drop in the H_2S content of the ore fluids. Other factors that may have enhanced gold deposition include reduction of the ore fluid, as suggested by alteration assemblages around gold bearing veins, phase separation or fluid mixing (e.g., Huston and Large 1989; Mikucki and Groves 1990; Arcos et al. 1991; Hayashi and Ohmoto 1991; Gammons and William-Jones 1995).

Phases two to four: remobilization during D_3, D_4, and D_5

The second fluid phase coincided with peak metamorphism and produced syn-D_3 sulfides and D_3 quartz, quartz-carbonate, and calcite veins. Textural evidence suggests that metamorphic remobilization of syn-D_1 sulfides produced the syn-D_3 sulfides, although sulfur isotope data suggest possible introduction of new sulfur.

The third fluid phase involved the formation of D_4 quartz and calcite veins and the post-D_3 sulfides that are found within the veins. Carbon for the calcite veins was probably sourced from preexisting carbonate in the form of calcite veins and/or possible carbonate facies BIF.

Remobilization of gold during D_3 and D_4 may have involved chloride complexing, as D_3 fluids coincided with peak metamorphism (600°C) and fluid inclusions indicate that the D_4 fluid was highly saline and CO_2-poor. The D_4 fluid was also H_2S-poor, as there was only minor deposition of sulfides. The final hydrothermal phase involved only minor D_5 calcite veins with minor sulfides.

Acknowledgements This research was funded by an ARC grant to R.A.B. and provision of a Ph.D. scholarship to G.J.A. by North Flinders Mines (now Newmont). Many North Flinders Mines geologists contributed by way of helpful discussion and suggestions; in particular, T. Ireland and G. Bosch are thanked for their support and encouragement throughout the study. The laser Raman analyses were made possible by the cooperation of T. Mernagh of Geoscience Australia, and A. Boyce, T. Fallick, and A. Tait generously made available the equipment at SUERC to enable R.A.B. to carry out some sulfur isotope analyses by laser ablation. Maria Adams is thanked for her patient drafting of the figures, which we continuously altered. We would also like to thank Ian Scrimgeour and Howard Poulsen for their constructive reviews of the manuscript. David Huston polished the final manuscript for publication.

References

Adams GJ (1997) Structural evolution and ore genesis of The Granites gold deposits, Northern Territory. PhD thesis. University of Adelaide

Arcos D, Soler A, Ayora C (1991) Gold transport conditions in shear zones from the Central Pyrenees, Spain. In: Pagel M, Leroy JL (eds) Source, transport and deposition of metals. Balkema, Rotterdam, pp 633–636

Barker AJ (1990) Introduction to metamorphic textures and microstructures. Blackie, London

Bell AM (1981) Vergence: an evaluation. J Struct Geol 3:197–202

Bloem EJM, Dalstra HJ, Groves DI, Ridley JR (1994) Metamorphic and structural setting of Archaean amphibolite-hosted gold deposits near Southern Cross, Southern Cross Province, Yilgarn Block, Western Australia. Ore Geol Reviews 9:183–208

Böhlke JK (1989) Comparison of metasomatic reactions between a common CO_2-rich vein fluid and diverse wall rocks: intensive variables, mass transfers and Au mineralization at Alleghany, California. Econ Geol 84:291–327

Burrows DR, Spooner ETC, Wood PC, Jemielita RA (1993) Structural controls on formation of the Hollinger–McIntyre Au quartz vein system in the Hollinger Shear Zone, Timmins, southern Abitibi greenstone belt, Ontario. Econ Geol 88:1643–1663

Colvine AC, Fyon JA, Heather KB, Marmont S, Smith PM, Troop DG (1988) Archean lode gold deposits in Ontario. Ontario Geol Surv Misc Paper 139, 136 pp

Cooper JA, Ding PQ (1997) Zircon ages constrain the timing of deformation events in the The Granites–Tanami region, northwest Australia. Aust J Earth Sci 44:777–787

Crispe AJ, Vandenberg LC, Scrimgeour IR (2006) Geological framework of the Palaeoproterozoic Tanami Region, Northern Territory. Miner Depos (this issue)

Davidson GJ, Large RR, Kary GL, Osborne R (1989) The deformed iron-formation-hosted Starra and trough tank Au–Cu mineralisation: a new association from the Proterozoic eastern succession of Mount Isa, Australia. Econ Geol Mon 6:135–150

Davis DW, Lowenstein TK, Spencer RJ (1990) Melting behaviour of fluid inclusions in laboratory-grown halite crystals in the systems NaCl–H_2O, NaCl–KCl–H_2O, NaCl–$MgCl_2$–H_2O, and NaCl–$CaCl_2$–H_2O. Geochim Cosmochim Acta 54:591–601

Ding P, Giles C (1993) Geological setting of gold mineralisation in the Tanami region, Northern Territory, Australia. Proceedings of the International Symposium on Gold Mining Technology, Beijing, June 1993, pp 15–17

Etheridge MA, Rutland RWR, Wyborn LAI (1987) Orogenesis and tectonic process in the Early to Middle Proterozoic of Northern Australia. In: Kroner A (ed) Proterozoic lithospheric evolution. Geodynamic Ser. 17, Am Geophys Union, Washington DC, pp 131–147

Ettner DC, Bjorlykke A, Andersen T (1994) A fluid inclusion and stable isotope study of the Proterozoic Bidjovagge Au–Cu deposit, Finnmark, northern Norway. Miner Depos 29:16–29

Fedorowich J, Stauffer M, Kerrich R (1991) Structural setting and fluid characteristics of the Proterozoic Tartan Lake gold deposit, Trans-Hudson Orogen, Northern Manitoba. Econ Geol 86:1434–1467

Gammons CH, William-Jones AE (1995) The solubility of Au–Ag alloy + AuCl in HCl/NaCl solutions at 300°C: new data on the salinity of Au(I) chloride complexes in hydrothermal fluids. Geochim Cosmochim Acta 59:3453–3468

Garnaut K (1995) Geochemical classification of the mafics in The Granites–Tanami inlier and their implications for the regions evolution. Unpubl. Hons. thesis, University of Adelaide, Australia

Giles AD, Marshall B (1994a) Fluid inclusion studies on a multiply deformed metamorphosed volcanic-associated massive sulfide deposit, Joma Mine, Norway. Econ Geol 89:803–819

Giles AD, Marshall B (1994b) The misidentification and misuse of fluid inclusions in studies of metamorphosed and deformed ore deposits. Geol Soc Aust Abstr 37:130

Giles AD, Marshall B (1995) The misuse of fluid inclusions in deformed metamorphosed and metamorphogenic (pre- and syn-tectonic) ore deposits. In: Pasava, Kríbek, Zák (eds) Mineral deposits. Balkema, Rotterdam, pp 865–868

Groves DI, Phillips GN, Falconer LJ, Houstoun SM, Ho SE, Browning P, Dahl N, McNaughton NJ (1987) Evidence for an epigenetic origin for BIF-hosted gold deposits in greenstone belts of the Yilgarn Block, Western Australia. In: Ho SE, Grove DI (eds) Recent advances in understanding Precambrian gold deposits. Geol. Dept. and Uni. Ext., University of Western Australia 11:167–179

Harley M, Charlesworth EG (1990) Structural controls in the distribution of gold at the How Mine, Bulawayo, Zimbabwe. Econ Geol 85:1697–1710

Hayashi K-I, Ohmoto H (1991) Solubility of gold in NaCl- and H_2S-bearing aqueous solutions at 250–350°C. Geochim Cosmochim Acta 55:2111–2126

Hodgson CJ (1989a) Patterns of mineralisation. In: Bursnall JT (ed) Mineralisation and shear zones. Geol Assoc Can, Short Course 6:51–88

Hodgson CJ (1989b) The structure of shear-related, vein-type gold deposits: a review. Ore Geol Rev 4:231–273

Huston DL, Large RR (1989) A chemical model for the concentration of gold in volcanogenic massive sulphide deposits. Ore Geol Rev 4:171–200

Ibrahim MS, Kyser TK (1991) Fluid inclusions and isotope systematics of the high-temperature Proterozoic Star Lake Lode gold deposit, Northern Saskatchewan, Canada. Econ Geol 86:1468–1490

Ireland TJ, Mayer TE (1984) The geology and mineralisation of The Granites gold deposits, Northern Territory. Proceedings of Aus. I. M.M. Conference, Darwin, N.T. pp 397–405

Kelley SP, Fallick AE (1990) High precision spatially resolved analyses of $\delta^{34}S$ in sulphides using a laser extraction technique. Geochim Cosmochim Acta 54:883–888

Kerrich R (1989) Geodynamic setting and hydraulic regimes: shear zone hosted mesothermal gold deposits. In: Bursnall JT (ed) Mineralisation and shear zones. Geol Assoc Can, Short Course 6:89–128

Larocque ACL, Hodgson CJ, Lafleur P-J (1993) Gold distribution in the Mobrun volcanic-associated massive sulfide deposit, Noranda, Quebec: a preliminary evaluation of the role of metamorphic remobilisation. Econ Geol 88:1443–1459

Lhotka PG, Nesbitt BE (1989) Geology of unmineralized and gold-bearing iron formation, Contwoyto Lake–Point Lake region, Northwest Territories, Canada. Can J Earth Sci 26:46–64

Mayer TE (1990) The Granites gold field. In: Hughes FE (ed) Geology of the mineral deposits of Australia and Papua New Guinea. Aust Ints Min Metall Mon 14:719–724

Mernagh TP, Wygralak AS (2006) Ore fluids of the Tanami region. Miner Depos (this issue)

Mikucki EJ, Groves DI (1990) Gold transport and depositional models. In: Ho SE, Groves DI, Bennett JM (eds) Gold deposits of the Archaean Yilgarn Block, Western Australia: nature, genesis and exploration guides. Geol Dept and Uni Ext, University of Western Australia 20:278–284

Page RW (1988) Geochronology of Early to Middle Proterozoic fold belts in northern Australia: a review. Precamb Res 40/41:1–19

Page R, Sun S-s, Blake D (1995) Geochronology of an exposed late Archaean basement terrane in the Granites–Tanami region. AGSO Res Newsl 22:19–20

Phillips GN, Groves DI, Martyn JE (1984) An epigenetic origin for Archaean banded iron-formation hosted gold deposits. Econ Geol 79:162–171

Potter RW, Clyne MA, Brown DL (1978) Freezing point depression of aqueous sodium chloride solutions. Econ Geol 73:284–285

Ramsay JG (1967) Folding and fracturing of rocks. McGraw-Hill book Company, New York

Robert F (1990) Structural setting and control of gold–quartz veins of the Val d'Or area, southeastern Abitibi subprovince. In: Ho SE, Robert F, Groves DI (eds) Gold and base-metal mineralisation in the Abitibi subprovince, Canada, with emphasis on the Quebec segment. Geol Dept and Uni Ext, University of Western Australia. Australia 24:167–209

Robert F, Brown AC (1986a) Archean gold-bearing quartz veins at the Sigma Mine, Abitibi greenstone belt, Quebec: Part I. Geologic relations and formations of the vein system. Econ Geol 81:578–592

Robert F, Brown AC (1986b) Archean gold-bearing quartz veins at the Sigma Mine, Abitibi greenstone belt, Quebec: Part II. Vein paragenesis and hydrothermal alteration. Econ Geol 81:593–616

Robert F, Poulsen KH, Dube B (1994) Structural analysis of lode gold deposits in deformed terranes. Geol Surv Canada, Open File 2850

Roberts RG (1988) Archaean lode gold deposits. In: Roberts RG, Sheahan PA (eds) Ore deposit models. Geol Assoc Canada, Reprint Series 3:1–19

Robinson BW, Kusakabe M (1975) Quantitative preparation of sulfur dioxide, for $^{34}S/^{32}S$ analyses, from sulfides by combustion with cuprous oxide. Anal Chem 47:1179–1181

Roedder E (1984) Fluid inclusions. Reviews in Mineralogy 12

Rye DM, Rye RO (1974) Homestake gold mine, South Dakota: I Stable isotope studies. Econ Geol 69:293–317

Scott J (1993) The structural setting of Proterozoic gold mineralisation of the Bunkers Hill Open Cut Mine, The Granites, Northern Territory. Unpubl. Hons. thesis, University of Adelaide, Australia

Scrimgeour I, Sandiford M (1993) Early Proterozoic metamorphism at The Granites gold mine, Northern Territory: implications for the timing of fluid production in high-temperature, low-pressure terranes. Econ Geol 88:1099–1113

Smith JB (2001) Summary of results—Joint NTGS–AGSO Age Determination Program 1999–2001. Northern Territory Geol Surv Record 2001-007

Treagus SH (1988) Strain refraction in layered systems. J Struct Geol 10:517–527

Valenta R, Wall V (1996) Controls on gold mineralisation at The Granites, Tanami Desert, Northern Territory. Geol Soc Aust Abs 41:451

Vandenberg LC, Hendrickx MA, Crispe AJ, Slater KR, Dean AA (2001) Structural geology of the Tanami region. Northern Territory Geol Surv Record 2001-004

Vityk MO, Bodnar RJ (1995) Textural evolution of synthetic fluid inclusions in quartz during re-equilibration, with applications to tectonic reconstruction. Contrib Mineral Pet 121:309–323

Wygralak AS, Mernagh TP, Fraser G, Huston DL, Denton G, McInnes B, Crispe A, Vandenberg L (2001) Gold mineral systems in the Tanami region: new insights from NTGS–AGSO research. AGSO Res Newsl 34:2–14